DOI 10.24425/aee.2021.136993

An approach to suppress high-frequency resonance using model predictive and selective harmonic elimination combined strategy

SITONG CHEN, XIAOQIANG CHEN, YING WANG, YE XIONG

School of Automation and Electrical Engineering, Lanzhou Jiaotong University
Lanzhou, China
e-mail: sitong_chen@163.com

(Received: 06.08.2020, revised: 11.01.2021)

Abstract: High-frequency resonance is a prominent phenomenon which affects the normal operation of the high-speed railway in China. Aiming at this problem, the resonance mechanism is analyzed first. Then, model predictive control and selective harmonic elimination pulse-width modulation (MPC-SHEPWM) combined control strategy is proposed, where the harmonics which cause the resonance can be eliminated at the harmonic source. Besides, the MPC is combined to make the current track the reference in transients. The proposed control has the ability to suppress the resonance while has a faster dynamic performance comparing with SHEPWM. Finally, the proposed MPC-SHEPWM is tested in a simulation model of CRH5 (Chinese Railway High-speed), EMUs (electric multiple units) and a traction power supply coupled system, which shows that the proposed MPC-SHEPWM approach can achieve the resonance suppression and shows a better dynamic performance.

Key words: CRH5 EMUs and traction power supply coupled system, high-frequency oscillation, high speed railway, model predictive control (MPC), selective harmonic elimination pulse-width modulation (SHEPWM)

1. Introduction

High-frequency resonance has been frequently reported worldwide, which has a serious impact on the safety of the electric railway operation [1–4]. Sinusoidal pulse-width modulation (PWM) technology has been applied in electric vehicles for more than 20 years. There are high-frequency harmonics produced by PWM in these vehicles, which are injected into the traction network. When the high frequency harmonic injected into the traction network is the resonance frequency of the

traction power supply system, the resonance occurs [5–7]. In recent years, high-speed railways have rapidly developed in China, large quantities of AC–DC–AC drive multiple units (EMUs) using PWM converter technology have been put into operation, and the resonance phenomenon occurs more and more often. In 2007, the Beijing-Harbin railway line was put into operation, there have been four resonance overvoltage accidents which caused failures of the converter in EMUs. In 2011, the resonance overvoltage accident happened to the Beijing-Shanghai railway line. In 2017, the Beijing-Guangdong railway line suffered voltage fluctuation, as shown in Fig. 1, which caused the tripping of the main breaker in a traction substation. These phenomena are caused by the harmonics resonance which makes aware that resonance suppression scheme should be valued.

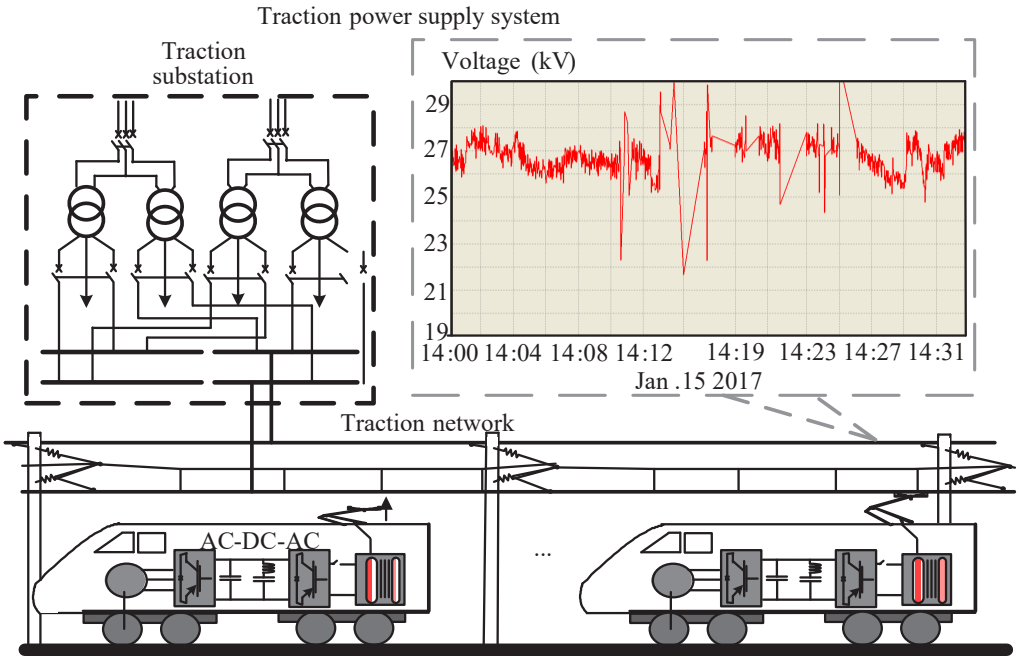

Fig. 1. Field measurement of high-frequency resonance in the Beijing-Guangdong railway line in China

Aiming at high-frequency resonance issues, some researchers have studied the influencing factors caused by the factors of a traction network, the positions, the running conditions, and the power of the vehicles [8–11]. In [12, 13], high-pass passive filters are installed in a traction power supply system (TPSS), where most of the high-frequency harmonics in the traction network can be filtered. Active power filters can be used on board vehicles and on the traction network to compensate for harmonics [14]. The resonance suppression is achieved in these studies by introducing filtering devices. Some scholars realize the suppression of the resonance without an extra filtering device, the adapted delta modulation strategy is adopted in the converter control to reduce the resonance harmonics injected to the TPSS, as documented in [15]. Some researchers brought forward the method of avoiding the resonant frequency harmonic generation, the selec-

tive harmonic elimination PWM (SHE–PWM) is used to suppress the resonance phenomenon. A novel in-phase disposition SPWM pulse allocation strategy applied to a cascaded H-bridge (HB) converter is presented in [16], which lowers the total harmonic distortion (THD) of the voltage. In [17], resonant harmonic elimination PWM is proposed to suppress the resonance in a high-speed railway. A windowed SHWPWM control method is introduced for resonance suppression in [18], which makes the windowed design and the precalculated solutions to cover a wider potential resonant frequency range.

SHEPWM is a synchronous and symmetrical PWM with the advantages of low switching frequency, the high quality of the output waveform, etc. The output voltage of the converter is performed by the Fourier transform in SHEPWM, which is to solve the transcendental equation with the goal of eliminating harmonics and obtain an off-line switching table [19]. However, the SHEPWM waveform generated by looking up the switching table would lead to the weak dynamic response. Due to the variation of the operating condition in the TPSS, the different operating state of the vehicle leads variable traction load, it requires quick dynamic response in the control of the rectifier. The MPC (model predictive control) is a new optimization algorithm with good dynamin performance in the field of power electronic. In 2004, the finite control set model predictive control (FCS–MPC) was proposed by Chilean scholars according to which the switching state can be selected in an optimization problem. In this case, all the possible switching states are evaluated in the cost function, the switching states that minimize the cost function are selected. It allows one to achieve fast dynamic response at low switching frequency [20]. In [21], the FCS–MPC combined with SHWPWM control is proposed for a three-phase three-level HB converter, and the output waveform of the converter has the harmonic elimination characteristics of SHEPWM and the fast dynamic response of MPC.

In this paper, the MPC and SHEPWM combined (MPC-SHEPWM) strategy is used to solve phenomena of resonance, where the difference between the SHEPWM switching state and the candidate switching state and the output current error are taken as the optimization objectives of the MPC, so that the output waveform has the characteristics of harmonic elimination in SHEPWM and the characteristics of fast dynamic response in the MPC. First, the mathematic models of an auto-transform (AT) traction power network and China Railway Highspeed5 (CRH5) EMUs are established, and the high-frequency resonance mechanism of the TPSS is analyzed. Based on the mechanism, a MPC-SHEPWM control strategy is proposed to eliminate the resonant harmonics in CRH5 and achieve the potential high-frequency resonance suppression in high-speed railways. Besides, a simulation model of the dual four-quadrant pulse rectifier in CRH5 is established and the dynamic performances of SHEPWM and MPC-SHEPWM are compared. Finally, a CRH5-EMUs-TPSS model is established to verify the effectiveness and the reliability of the proposed control strategy for high-frequency resonance suppression.

2. Resonance mechanism traction power supply system

The TPSS in China is an all-parallel AT-fed power supply system with single-phase AC power and electrical parameters of 2×27.5 kV 50 Hz, there is a coupling relationship of mutual impedance and a stray capacitor between conductors of each line. In order to analyze the harmonic characteristics of the traction power supply system, the T-type equivalent circuit is established

respectively for the transmission line on both sides of the vehicle, as it is shown in Fig. 3. Z_o is the equivalent impedance of the power supply facilities and the transmission line on the other side of the facilities, respectively, Z_{L1}, Z_{L2} and Y_{L1}, Y_{L2} are the equivalent impedance and admittance of the left-side and right-side transmission line seen from the harmonic source, respectively.

When the equivalent impedance of the left side and the right side of the vehicle is capacitive and inductive respectively, there is resonant frequency causing the parallel resonance to occur. In order to analyze the parallel resonance, the CRH5 EMUs can be equivalent to a current harmonic source I_N [23], which generates a number of odd number higher harmonics, literature [22] has analyzed the harmonic characteristics of the two-level four quarant pulse rectifier (4QPR). When the harmonic of I_N injected into the traction network is equal to the resonant frequency, the resonance would occur.

In Fig. 2, the input impedance Z_i of the traction network seen from EMUs can be calculated as:

$$Z_i = \frac{Z_c \cosh \gamma(l - l_1) \times (Z_o \cosh \gamma l_1 + + Z_c \sinh \gamma l_1)}{Z_o \sinh \gamma l + Z_c \cosh \gamma l}, \tag{1}$$

where: $l = l_1 + l_2$ is the total length of the transmission line, l_1, l_2 are the left-side length and the right-side length, respectively. Z_i is the characteristic impedance of the transmission line, $\gamma = \sqrt{ZY}$ is the propagation constant, Z and Y are the equivalent impedance and admittance per unit length of the transmission line, respectively.

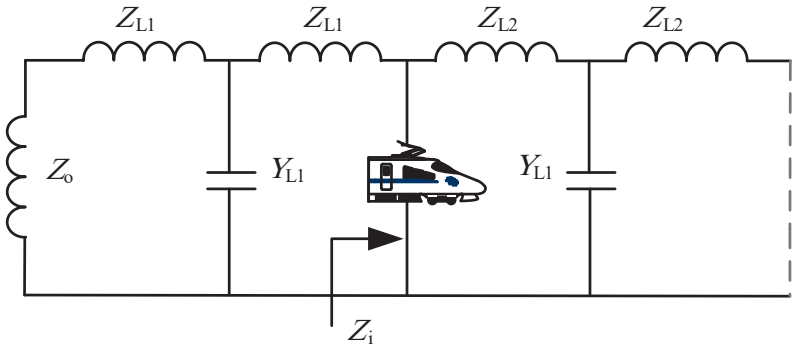

Fig. 2. Vehicle-traction power supply coupled system

When the resonance occurs, Z_i would attain the maximum value, so that the denominator in (1) would approach zero.

$$Z_o \sinh \gamma l + Z_c \cosh \gamma l = 0, \tag{2}$$

where: $\gamma l < 1$, so that $\tan \gamma l \approx \gamma l$, $Z_o = \omega L_o = -Z_c/(\gamma l)$.

At this point, the resonant frequency can be expressed as:

$$f_{rp} = 1/(2\pi\sqrt{L_o C}), \tag{3}$$

where C represents the equivalent inductance and the capacitance of Y.

3. Proposed model of predictive selective and harmonic elimination combined strategy

The proposed control schematic is shown in Fig. 3, the control under dq frame of the dual four-quadrant pulse two-level rectifier is adopted in CRH5 EMUs [24]. Because the rectifier is a single-phase one in EMUs, the voltage and current of the AC side are regarded as components in the α frame, and the imaginary voltage and current in the β frame should be fabricated. Then the voltage and current are transferred to the dq coordinate system through the Park transformation, so that the AC signal can be transformed into the DC signal. The DC voltage can be achieved by controlling the voltage in an outer loop and zero reactive power can be achieved by controlling the relationship of variables in the dq system. The control under dq frame is continued to be adopted in the proposed MPC-SHEPWM.

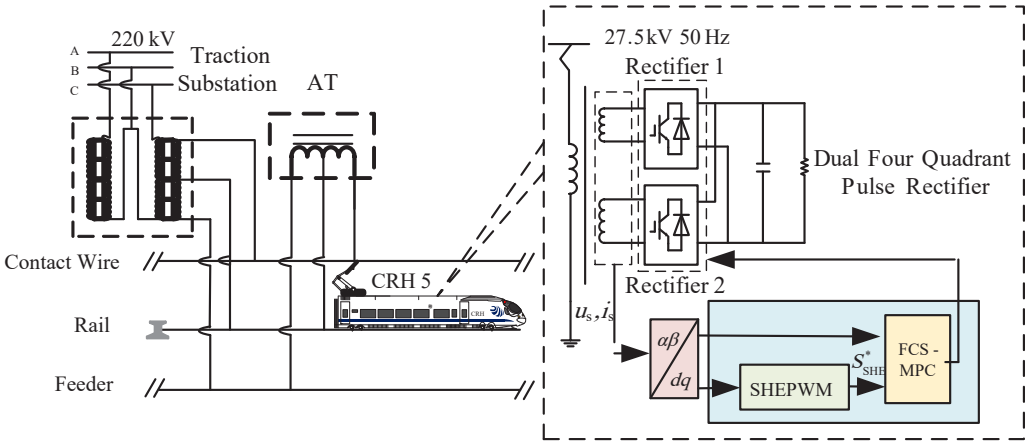

Fig. 3. Control schematic of MPC-SHEPWM for a single-phase CRH5 EMUs rectfier

To realize the suppression of the high-frequency resonance, SHEPWM is designed first and the switching signals S^*_{SHE} of PWM is obtained in 3.1. However, there is a weakness of the dynamic performance in SHEPWM, aiming at this issue, the FCS–MPC is introduced in 3.2 to make up for the weakness, where there is an advantage of fast dynamic performance. The switching signals S^*_{SHE} in SHEPWM is added as constraints in the cost function in the FCS–MPC in 3.3 to make it combined, and the performance of resonance suppressing and fast dynamic can be realized.

3.1. Selective harmonic elimination PWM

Reference [23] made theoretical analysis and introduction of the SHEPWM technology, which can control the fundamental and harmonic waveform by adjusting the positions of the switching angle.

The two-level rectifier is adopted in CRH5 EMUs, as shown in Fig. 4, there are N switching angles in a quarter period, SHEPWM requires the waveform to have the characteristics of a quarter-period symmetry waveform, in this way, the even-order harmonic component and zero-order

component are naturally eliminated as well as the amplitude of the fundamental component and harmonic components.

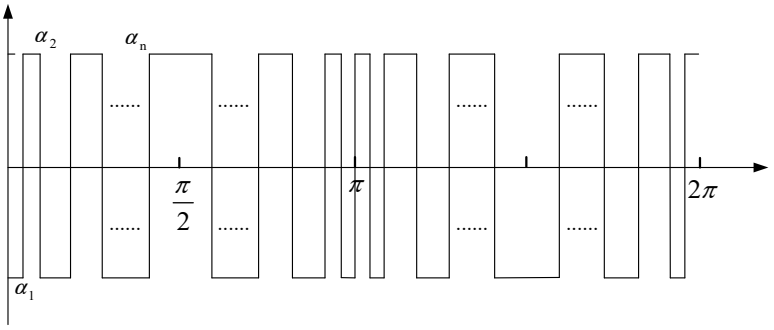

Fig. 4. Two-level pulse waveform

b_n is the amplitude of the $n-$th order, the $n-$th harmonic can be eliminated by setting b_n to zero. For the two-level rectifier, the expression of b_n can be expressed as follows:

$$b_n = \sum_{i=1}^{N} (-1)^{i-1} \cos(n\alpha_i). \tag{4}$$

The switching frequency of CRH5 EMUs is 250 Hz, so that there are five controllable switching angles in a quarter period, as for the dual rectifier, there are 10 controllable switching angles. The control of the fundamental wave of rectifier 1 and rectifier 2 is independent, while the control of the harmonic is achieved by the control of a synthesized PWM waveform. The fundamental frequency can be written as:

$$\left(\sum_{i=1}^{5} (-1)^{i-1} \cos(\alpha_i) - M\right)^2 + \left(\sum_{i=6}^{10} (-1)^{i} \cos(\alpha_i) - M\right)^2 = 0. \tag{5}$$

$M \in (0.5, 1.0)$ is the modulation index which is governed by:

$$M = \frac{\pi}{4u_{\mathrm{dc}}} b_1\,, \tag{6}$$

where: b_1 is the fundamental component, u_{dc} is the DC voltage of the rectifier, and the constraint of the switching angles α_i is:

$$\begin{cases} 0 < \alpha_1 < \alpha_2 < \alpha_3 < \alpha_4 < \alpha_5 < \dfrac{\pi}{2} \\ 0 < \alpha_6 < \alpha_7 < \alpha_8 < \alpha_9 < \alpha_{10} < \dfrac{\pi}{2} \end{cases}. \tag{7}$$

The harmonic elimination control can be realized by:

$$\left(\sum_{i=1}^{5} (-1)^{i-1} \cos(n\alpha_i) + \sum_{i=6}^{10} (-1)^{i-1} \cos(n\alpha_i)\right) = 0. \tag{8}$$

Among 10 controllable switching angles, two are used to control the fundamental components of rectifiers, so that up to 8 harmonics can be controlled. In this paper, the resonance frequency of the traction network supply system is 1550 Hz, since the even harmonics are not contained in the symmetrical pulse waveform, the higher harmonics n are selected as 27-th, 29-th, 31-th, 33-th, and the remaining harmonics are lower harmonics, they are 3-th, 5-th, 7-th, 23-th. For transcendental equations with many dimensions and constraints, there may be no solutions under these conditions, so that (7) and (8) can be described as nonlinear optimization functions.

$$F_{\min} = \left(\sum_{i=1}^{5}(-1)^{i-1}\cos(\alpha_i) - M\right)^2 + \left(\sum_{i=6}^{10}(-1)^{i}\cos(\alpha_i) - M\right)^2 + \\ + \left(\sum_{i=1}^{5}(-1)^{i-1}\cos(n\alpha_i) + \sum_{i=6}^{10}(-1)^{i-1}\cos(n\alpha_i)\right). \tag{9}$$

Due to the complexity of the calculations, it can be performed offline with different algorithms such as Newton's iteration, the Walsh function method, particle swarm optimization and biogeographical based optimization [24–27]. The Newton iteration method is adopted in this paper to calculate ten sets of switching angles as showed in Fig. 5, so that the requiring angles can be obtained according to M with a look-up table, then the switching angles can be converted into the switching driving signals S^*_{SHE} of traction rectifier bridge arms.

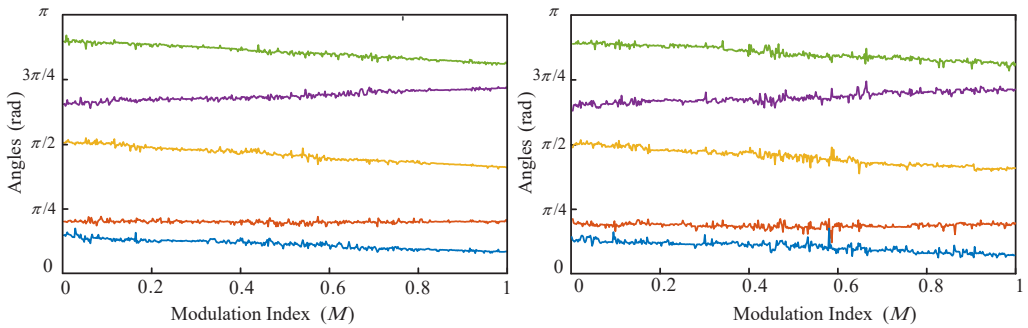

Fig. 5. Sets of solutions of SHEPWM switching angles α_1–α_5 (a); SHEPWM switching angles α_6–α_{10} (b)

3.2. FCS–MPC applied in PWM

Fig. 6 depicts the four-quadrant pulse rectifier used in CRH5 EMUs. R_{d} and C_{d} stand for the equivalent impedance supporting capacitor in the DC link, respectively, u_{dc} is the voltage in the DC link, u_{s} and i_{s} are the voltage and current of the rectifier of the traction network side, respectively, R_{s} represents the equivalent resistance, L_{s} is the inductance of the rectifier. In Fig. 6, the mathematical state equation of each part of the dual rectifier can be expressed as:

$$L\frac{\mathrm{d}i_{\mathrm{s}}}{\mathrm{d}t} = u_{\mathrm{s}} - R_{\mathrm{s}}i_{\mathrm{s}} - u_{\mathrm{ab}}\,. \tag{10}$$

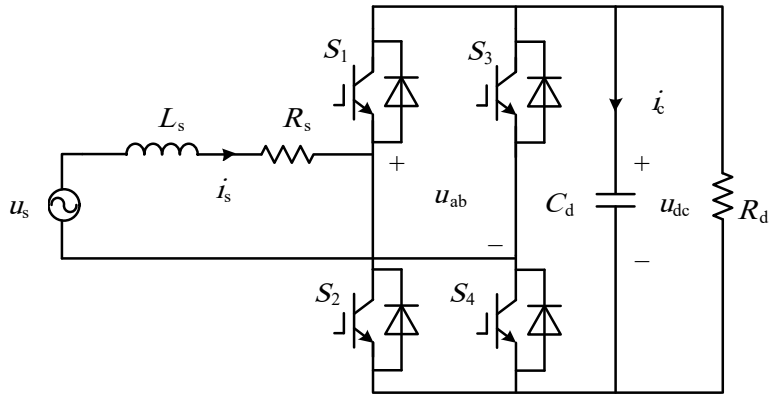

Fig. 6. Two-level four-quadrant pulse rectifier in CRH5 EMUs

The value of R_s is small and can be ignored, the mathematical model of the rectifier in the rotating dq coordinate can be derived as in (11).

$$\begin{cases} u_{abd} = u_{sd} - L\dfrac{\mathrm{d}i_{sd}}{\mathrm{d}t} + \omega L i_{sq} \\ u_{abq} = u_{sq} - L\dfrac{\mathrm{d}i_{sq}}{\mathrm{d}t} - \omega L i_{sd} \end{cases}, \tag{11}$$

where: i_{sd} and i_{sq} represent the currrent i_s decoupled in the dq system, u_{abd} and u_{abq} are the voltage u_s decoupled in the dq system.

In this paper, the FCS–MPC is operated in a discrete time with a sampling time and one step prediction horizon, the schematic of the FCS–MPC is shown as Fig. 7, where variables $x(k)$ represent the instantaneous value at the current hour kT_s, $x(k+1)$ is the predictive value at $(k+1)T_s$, S_{ab} is the switching function which is defined as:

$$S_{ab} \in \{1,\ 0,\ -1\}. \tag{12}$$

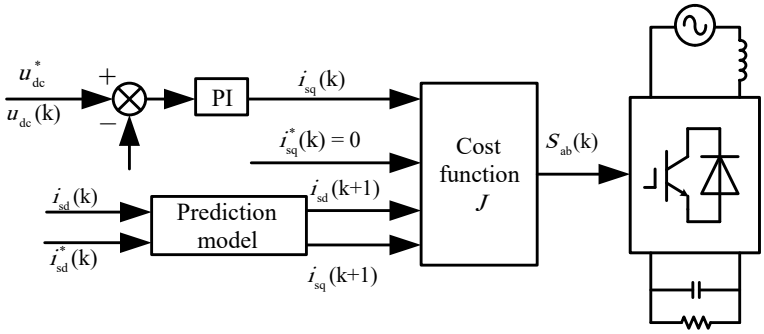

Fig. 7. Schematic of FCS–MPC strategy

At the beginning of the k-th sampling cycle, the current i_{sd} and i_{sq} are sampled firstly, then the prediction model is used to calculate the $(k+1)$-th prediction values under the three switching states S_{ab}, and the switching state that minimizes the cost function J is selected as the optimal state in (13).

$$S_{ab}(k) = \arg\{\min J(k)\}. \tag{13}$$

In order to calculate the prediction value, the discretization model of i_s in the dq frame can be expressed as:

$$\begin{cases} \left.\dfrac{\mathrm{d}i_{sd}}{\mathrm{d}t}\right|_{t=k} = \dfrac{i_{sd}(k+1)-i_{sd}(k)}{T_s} = \dfrac{u_{sd}(k)-S_{abd}(k)u_{dc}(k)}{L} + \omega i_{sq}(k) \\ \left.\dfrac{\mathrm{d}i_{sq}}{\mathrm{d}t}\right|_{t=k} = \dfrac{i_{sq}(k+1)-i_{sq}(k)}{T_s} = \dfrac{u_{sq}(k)-S_{abq}(k)u_{dc}(k)}{L} - \omega i_{sd}(k) \end{cases}. \tag{14}$$

According to (14), the predictive current $i(k+1)$ can be expressed as:

$$\begin{cases} i_{sd}(k+1) = i_{sd}(k) + \dfrac{T_s}{L}\left[u_{sd}(k) - S_{abd}(k)u_{dc}(k)\right] + \omega T_s i_{sq}(k) \\ i_{sq}(k+1) = i_{sq}(k) + \dfrac{T_s}{L}\left[u_{sq}(k) - S_{abq}(k)u_{dc}(k)\right] - \omega T_s i_{sd}(k) \end{cases}. \tag{15}$$

Formula (15) can be transformed into the α/β static coordinate as:

$$\begin{cases} i_{sd}(k+1) = i_{sd}(k) + \omega T_s i_{sq}(k) + \\ \qquad \dfrac{T_s}{u_{sd}(k)L}\left\{u_{sd}^2(k) - \left[u_{s\alpha}(k)S_{ab\alpha}(k) + u_{s\beta}(k)S_{ab\beta}(k)\right]u_{dc}(k)\right\} \\ i_{sq}(k+1) = i_{sq}(k) - \omega T_s i_{sd}(k) - \dfrac{T_s}{u_{sq}(k)L}\left[u_{s\beta}(k)S_{ab\alpha}(k) - u_{s\beta}(k)S_{ab\alpha}(k)\right] \end{cases}. \tag{16}$$

In the control system of a single-phase PWM rectifier, only the voltage $u_{ab\alpha}(k)$ is needed to achieve the system control, the obtained voltage vector $u_{ab\beta}(k)$ does not exist in the actual system, so that this virtual quantity can be discarded. Therefore, only the switching function $S_{ab\alpha}(k)$ is needed.

The control objective is to get accurate modulation wave of the rectifier $S_{ab\alpha}(k)$ by minimizing the error of the AC side current, so that the cost function J can be expressed as:

$$J = \left[i_{sd}^* - i_{sd}(k+1)\right]^2 + \left[i_{sq}^* - i_{sq}(k+1)\right]^2, \tag{17}$$

where i_{sd}^* and i_{sq}^* are the reference values of i_{sd} and i_{sq}. By substituting the cost function J and three switching states S_{ab} into (13), the optimal switching state can be obtained.

3.3. FCS–MPC integrated into SHEPWM

To achieve better performance of the rectifier control, extra items are normally added to the cost function [28], therefore, SHEPWM is added in MPC in this section, which is shown in Fig. 8.

The cost function can be designed as in (18),

$$J = \left[i_{sd}^* - i_{sd}(k+1)\right]^2 + \left[i_{sq}^* - i_{sq}(k+1)\right]^2 + \sigma(k)\left[S_{ab}(k) - S_{SHE}^*(k)\right]^2. \tag{18}$$

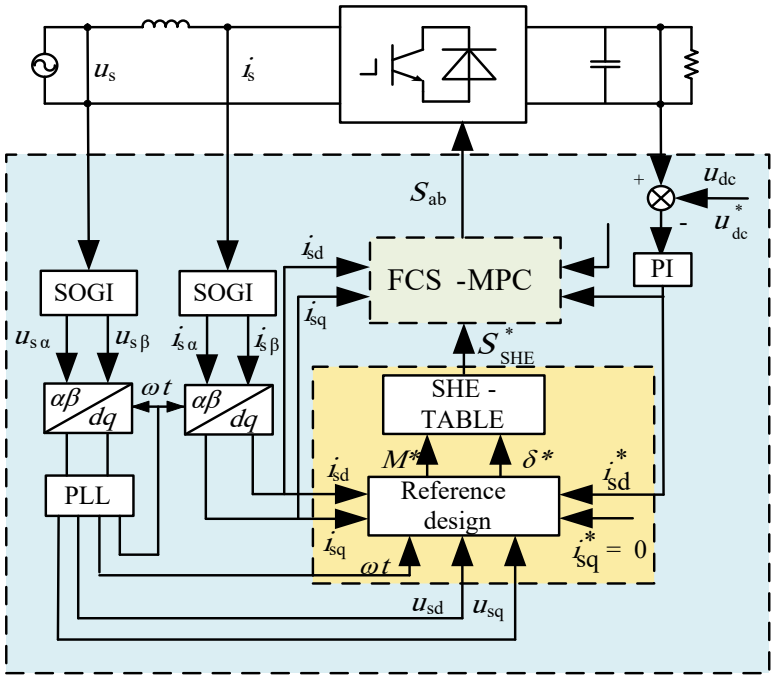

Fig. 8. Functional block diagram of the proposed MPC-SHEPWM

In (18), the first item is the basic control objective, which tracks the current of the AC side. The second item is a constraint item, and the weighting factor σ is introduced in, which constrains the switching action of the rectifier to fix the frequency spectrum of the PWM rectifier injected into the traction network. According to the SHEPWM algorithm proposed in Section 3.1, the corresponding voltage switching state S^*_{SHE} is used as the reference, because MPC is operated in a discrete time, $S^*_{\mathrm{SHE}}(t)$ should be discretized into $S^*_{\mathrm{SHE}}(k)$, where:

$$S^*_{\mathrm{SHE}}(k) = S^*_{\mathrm{SHE}}(M(k), \delta(k)). \tag{19}$$

The modulation index M^* should be determined to obtain the optimal angles α_i, and the switching states S^*_{SHE} can be obtained by comparing α_i, which is shown in Fig. 7, and the phase angle δ^* of the voltage u_s. The parameters M^* and δ^* under the dq frame are defined as:

$$M^* = \frac{\pi}{4u^*_{\mathrm{dc}}}\sqrt{\left(u^*_{\mathrm{abd}}\right)^2 + \left(u^*_{\mathrm{abq}}\right)^2}, \qquad \delta^* = \theta - \arctan\left(\frac{u^*_{\mathrm{abq}}}{u^*_{\mathrm{abd}}}\right). \tag{20}$$

Weighting factor σ is introduced in the second item, when a low value is chosen as σ, the control system tends to be a standard FCS–MPC current control system, where the dynamic response will be fast, but the switching frequency and the harmonic spectrum are difficult to guarantee. On the contrary, there will be better harmonic spectrum characteristics in the waveform of PWM if σ is high, but the dynamic response of the system will be slower. Considering the

control performance of both dynamic and steady performance, the weighting factor σ can be designed as:

$$\sigma(k) = \begin{cases} \sigma_{\max} - \Delta i(k), & \sigma(k) \geq \sigma_{\min} \\ \sigma_{\max}, & \sigma(k) < \sigma_{\min} \end{cases}, \tag{21}$$

where

$$\Delta i(k) = \frac{\left[i_{\mathrm{sd}}(k) - i^*_{\mathrm{sd}}(k)\right]^2 + \left[i_{\mathrm{sq}}(k) - i^*_{\mathrm{sq}}(k)\right]^2}{\left[i^*_{\mathrm{sd}}(k)\right]^2 + \left[i^*_{\mathrm{sq}}(k)\right]^2}. \tag{22}$$

$\sigma_{\max}$ and $\sigma_{\min}$ represent the upper limit and lower limit of the weighting factor σ, respectively. In the steady state, the restriction of output spectrum characteristics of PWM is designed as the main function of the controller because of less current deviation. In the dynamic state, the current deviation increases, the controller mainly realizes the current tracking.

After the entire possible voltage level is evaluated, the optimal converter switching function S_{ab} given by the proposed MPC-SHE can be carried out by minimizing the cost function.

4. Simulation and verification test

4.1. Dynamic performance test

A simulation model of dual four-quadrant pulse EMU rectifiers is built in Matlab/Simulink, the parameters are listed in Table 1.

Table 1. Parameter values of CRH5 EMU rectifier

Parameter	Symbol	Value	Unit
Primary side voltage of the transformer	U_{s}	27.5	kV
Equivalent resistance of the rectifier	R_n	0.145	Ω
Equivalent inductance of the rectifier	L_n	5.4	mH
DC-link voltage	u_{dc}	3600	V
DC-side equivalent resistance capacitance	C_{d}	10	mF
DC-side equivalent resistance	R_{d}	9	Ω
Sampling frequency of the simulation	f_{s}	10	kHZ
Weighting factor	$\sigma_{\min}$	0.01	/
Weighting factor	$\sigma_{\max}$	8.5	/

The SHEPWM pattern prevails in MPC-SHEPWM control, when a step-change in the current is applied at 1.0 s, as shown in Fig. 9(a), which produces an increment in the current relative deviation $\Delta i(k)$, the MPC pattern prevails, currents i_{sd} and i_{sq} quickly reach a new stable working state (about 0.018 s), and there is no overshoot in the adjusting process. In order to make a comparison, the same step-change is also used in PI-SHEPWM. There is no longer adjustment

time of the rectifier with PI-SHEPWM as shown in Fig. 9(b), which shows that MPC-SHWPEM performed a better dynamic performance.

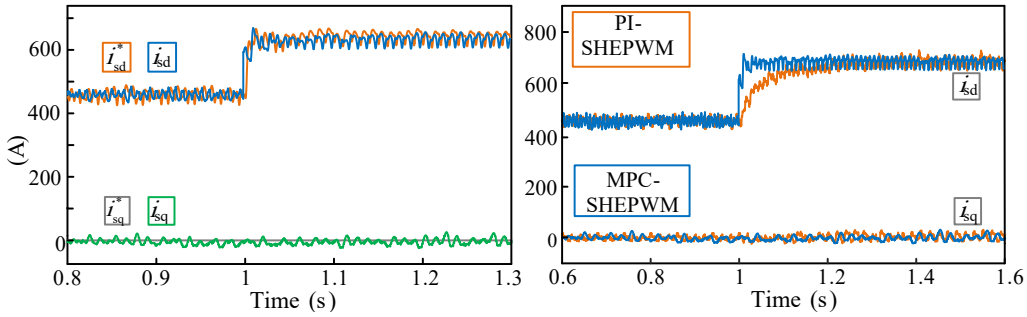

Fig. 9. Dynamic simulation results based on two control methods

4.2. Resonance suppressing test

The simulation model of a CRH5 EMUs-TPSS is built in MATLAB/Simulink, as shown in Fig. 10, the encapsulation module represents 15 km traction networks, one with subscript "1" is the upgoing line, and "2" is the downgoing line; subscripts "in" and "out" represent the input and output, respectively; T is the contact line, R is the rail, G is the connecting wire, F is the feeder line, and P represents the protection line.

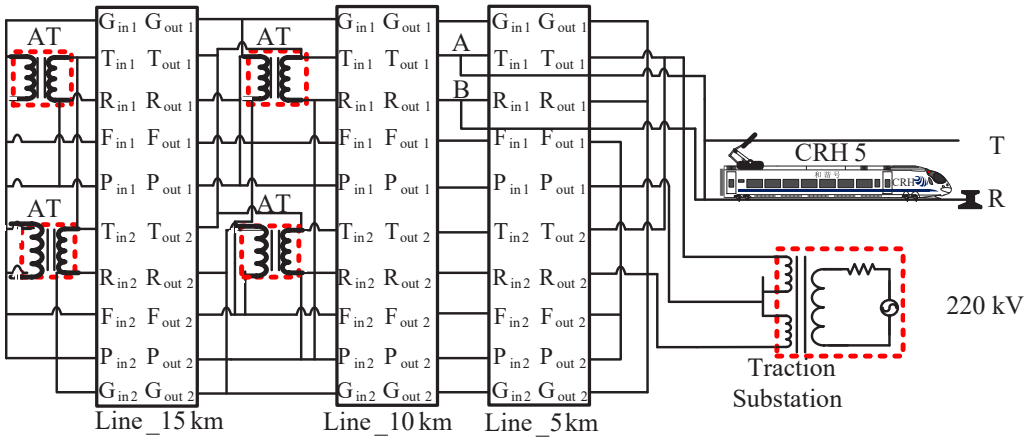

Fig. 10. Simulation model of CRH5 EMUs-TPSS

The impedance measurement under different frequencies is made for the traction power network model shown in Fig. 11, which shows that the impedance value is highest at a frequency of 1550 Hz nearby, so when a vehicle's current of about 1550 Hz enters the traction power network, it causes the resonance phenomenon of the traction power system.

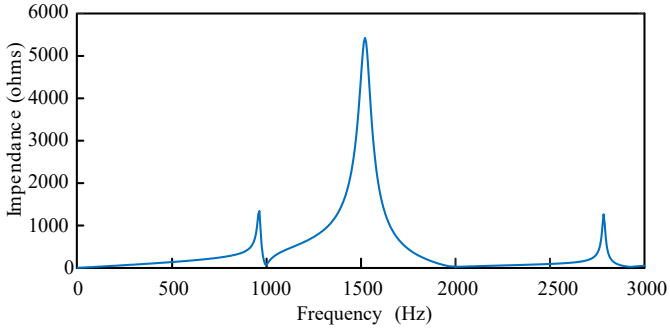

Fig. 11. Impedance measurement test result of traction power system

It can be seen from Fig. 12(c) that the harmonics of the pantograph current of CRH5 EMUs injected into the traction power network are concentrated around 31-th, which coincides with the resonant frequency stimulating the EMUs-TPSS resonance, the harmonics around 1550 Hz in the

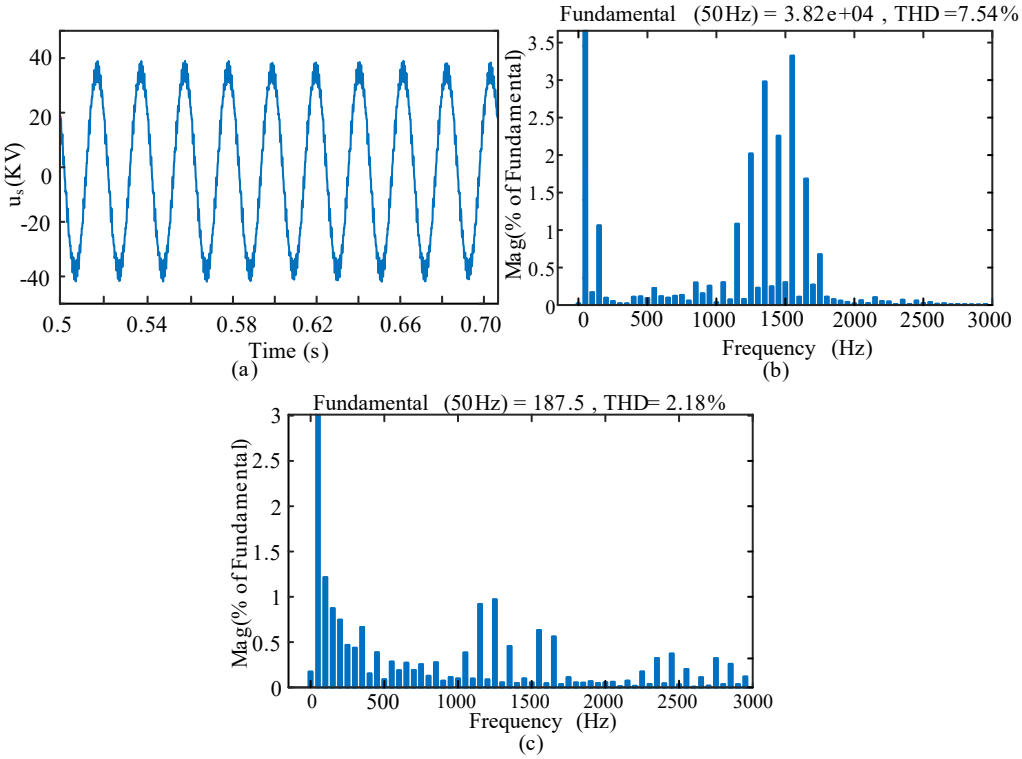

Fig. 12. Waveform and FFT spectrum with tractional control strategy: waveform of the voltage in traction power network(a); FFT spectrum of the voltage in traction power network (b); FFT spectrum of pantograph current (c)

voltage of the traction power network becomes rich, as shown in Fig. 12(b), and the the voltage of the traction network is amplified to 40 kV, which is shown in Fig. 12(a).

The resonance is suppressed by adopting the proposed MPC-SHEPWM, as shown in Fig. 13, the voltage in Fig. 13(a) is distorted less significantly than that of the traditional controller in Fig. 12(a), the harmonics from 1500 to 2000 are nearly eliminated. The THD of the pantograph current of CRH5 EMU voltage decreases to only 0.86%, and the voltage of the traction network decreases to only 0.62% as shown in Figs. 13(b) and (c).

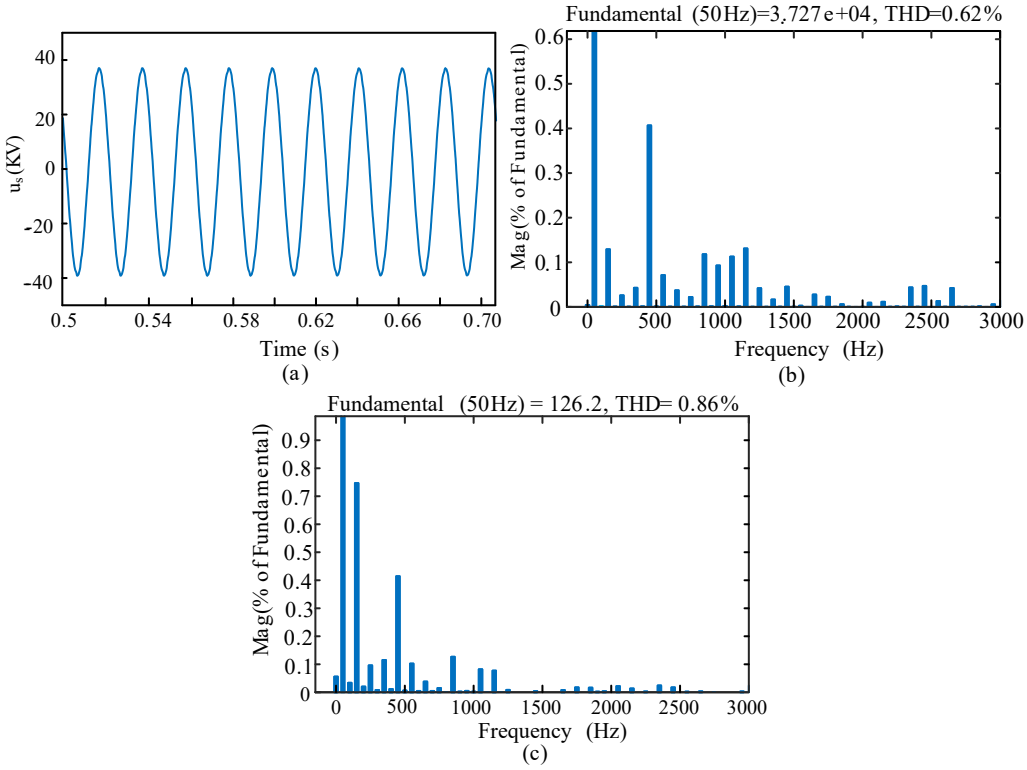

Fig. 13. Waveform and FFT spectrum with MPC-SHEPWM: waveform of the voltage in traction power network(a); FFT spectrum of the voltage in traction power network (b); FFT spectrum of pantograph current (c)

5. Conclusion

In this paper, aiming at the phenomenon of high-frequency resonance, the resonance mechanism is analyzed first. Based on the characteristic of a single-phase rectifier, the MPC-SHEPWM method is applied in the multiple 4QPR of CRH5 EMUs in China. Some conclusions can be drawn:

1) an MPC-SHEPWM controller has a better dynamic performance than a PI-SHEPWM controller,

2) the MPC-SHEPWM can suppress the characteristic harmonics of 3-th, 5-th, 7-th, 23-th, 27-th, 29-th, 31-th, 33-th,
3) the MPC-SHEPWM control can reduce the characteristic harmonics and THD of pantograph current and successfully suppress the high frequency resonance of the traction network voltage.

References

[1] Mollerstedt E., Bernhardsson B., *Out of control because of harmonics-an analysis of the harmonic response of an inverter locomotive*, IEEE Control Systems Magazine, vol. 20, no. 4, pp. 70–81 (2000).

[2] Sainz L., Caro M., Caro E., *Analytical Study of the Series Resonance in Power Systems With the Steinmetz Circuit*, IEEE Transactions on Power Delivery, vol. 24, no. 4, pp. 2090–2098 (2009).

[3] Lee H., Lee C., Jang G., Kwon S., *Harmonic analysis of the korean high-speed railway using the eight-port representation model*, IEEE Transactions on Power Delivery, vol. 21, no. 2, pp. 979–986 (2006).

[4] Holtz J., Kelin H., *The propagation of harmonic currents generated by inverter-fed locomotives in the distributed overhead supply system*, IEEE Transactions on Power Electronics, vol. 4, no. 2, pp. 168–174 (1989).

[5] Chang G.W., Lin H.W., Chen S.K., *Modeling characteristics of harmonic currents generated by high-speed railway traction drive converters*, IEEE Trans. Power Delivery, vol. 19, no. 2, pp. 766–773 (2004).

[6] Hu H., Shao Y., Tang L., Ma J., He Z., Gao S., *Overview of Harmonic and Resonance in Railway Electrification Systems*, IEEE Transactions on Industry Applications, vol. 54, no. 5, pp. 5227–5245 (2018).

[7] Kolar V., Palecek J., Kocman S. *et al.*, *Interference between electric traction supply network and distribution power network - resonance phenomenon*, International Conference on Harmonics and Quality of Power, Bergamo, Italy (2010).

[8] Brenna M. *et al.*, *Investigation of resonance phenomena in high speed railway supply systems: Theoretical and experimental analysis*, Elect. Power Syst. Res., vol. 81, no. 10, pp. 1915–1923 (2011).

[9] Hu H., Gao S., Shao Y., Wang K., He Z., Chen L., *Harmonic Resonance Evaluation for Hub Traction Substation Consisting of Multiple High-Speed Railways*, IEEE Transactions on Power Delivery, vol. 32, no. 2, pp. 910–920 (2017).

[10] Li J., Wu M., Molinas M., Song K., Liu Q., *Assessing High-Order Harmonic Resonance in Locomotive-Network Based on the Impedance Method*, IEEE Access, vol. 7, pp. 68119–68131 (2019).

[11] Hu H., Tao H., Blaabjerg F., Wang X., He Z., Gao S., *Train–Network Interactions and Stability Evaluation in High-Speed Railways–Part I: Phenomena and Modeling*, IEEE Transactions on Power Electronics, vol. 33, no. 6, pp. 4627–4642 (2018).

[12] Lee H., Kim G., Oh S., Lee C., *Optimal design for power quality of electric railway*, SICE-ICASE International Joint Conf., Busan, Korea, pp. 3864–3869 (2006).

[13] Hu H., He Z., Gao S., *Passive Filter Design for China High-Speed Railway With Considering Harmonic Resonance and Characteristic Harmonics*, IEEE Transactions on Power Delivery, vol. 30, no. 1, pp. 505–514 (2015).

[14] Zhang X., Chen J., Zhang G., Wang L., Qiu R., Liu Z., *An Active Oscillation Compensation Method to Mitigate High-Frequency Harmonic Instability and Low-Frequency Oscillation in Railway Traction Power Supply System*, IEEE Access, vol. 6, pp. 70359–70367 (2018).

[15] Holtz J., Krah J.O., *Suppression of time-varying resonances in the power supply line of AC locomotives by inverter control*, IEEE Transactions on Industrial Electronics, vol. 39, no. 3, pp. 223–229 (1992).

[16] Zhang Y., Xiong J., Kong L., Wang X., *A novel in-phase disposition SPWM pulse allocation strategy for cascaded H-bridge inverter*, Archives of Electrical Engineering, vol. 67, no. 2, pp. 361–375 (2018).

[17] Cui H., Song W., Fang H., Ge X., Feng X., *Resonant harmonic elimination pulse width modulation-based high-frequency resonance suppression of high-speed railways*, IET Power Electronics, vol. 8, no. 5, pp. 735–742 (2015).

[18] Song K., Konstantinou G., Mingli W., Acuna P., Aguilera R.P., Agelidis V.G., *Windowed SHE–PWM of Interleaved Four-Quadrant Converters for Resonance Suppression in Traction Power Supply Systems*, IEEE Transactions on Power Electronics, vol. 32, no. 10, pp. 7870–7881 (2017).

[19] Dahidah M.S.A., Konstantinou G., Agelidis V.G., *A Review of Multilevel Selective Harmonic Elimination PWM: Formulations, Solving Algorithms, Implementation and Applications*, IEEE Transactions on Power Electronics, vol. 30, no. 8, pp. 4091–4106 (2015).

[20] Rodriguez J. *et al*., *Predictive control of three-phase inverter*, Electronics Letters, vol. 40, no. 9, pp. 561–563 (2004).

[21] Aguilera R.P. *et al*., *Selective Harmonic Elimination Model Predictive Control for Multilevel Power Converters*, IEEE Transactions on Power Electronics, vol. 32, no. 3, pp. 2416–2426 (2017).

[22] Cui H., Feng X., Song W., *Modeling of high-order harmonic load for high-speed train*, Electr. Power Equip. Autom., vol. 33, no. 7, pp. 92–99 (2013).

[23] Dolara A., Gualdoni M., Leva S., *Impact of high-voltage primary supply lines in the* 2×25 *kV 50 Hz railway system on the equivalent impedance at pantograph terminals*, IEEE Transactions on Power Delivery, vol. 27, no. 1, pp. 164–175 (2012).

[24] Dahidah M.S.A., Konstantinou G., Agelidis V.G., *A Review of Multilevel Selective Harmonic Elimination PWM: Formulations, Solving Algorithms, Implementation and Applications*, IEEE Transactions on Power Electronics, vol. 30, no. 8, pp. 4091–4106 (2015).

[25] Liang T.J., Hoft R.G., *Walsh function method of harmonic elimination*, Proc. IEEE Appl. Power Electron. Conf., San Diego, CA, USA, Mar. 7–11, pp. 847–853 (1993).

[26] Yang K., Yuan Z., Yuan R., Yu W., Yuan J., Wang J., *A Groebner Bases Theory-Based Method for Selective Harmonic Elimination*, IEEE Transactions on Power Electronics, vol. 30, no. 12, pp. 6581–6592 (2015).

[27] Kavitha R., Thottungal Rani, *WHTD missisation in hybird multilvel inverter biogeographcial based Optimisation*, Archives of Electrical Engineering, vol. 63, no. 2, pp. 187–196 (2014).

[28] Rodriguez J. *et al*., *State of the Art of Finite Control Set Model Predictive Control in Power Electronics*, IEEE Transactions on Industrial Informatics, vol. 9, no. 2, pp. 1003–1016 (2013).